PROJECTILE IONIZATION OF HYDROGEN-LIKE OXYGEN AND FLUORINE IONS INCIDENT ON MOLECULAR HYDROGEN

by

TRACY NOLAN TIPPING

B.S., East Texas State University, 1984

A MASTER'S THESIS

submitted in partial fulfillment of the

requirements for the degree

MASTER OF SCIENCE

Department of Physics

KANSAS STATE UNIVERSITY
Manhattan, Kansas

1986

Approved by:

Patricia Richard
Major Professor

LD
2668
.T4
1936
.T56
c. 2

A11207 233582

TABLE OF CONTENTS

LIST OF FIGURES

LIST OF TABLES

ACKNOWLEDGEMENTS

I wish to express my sincere appreciation to Dr. Patrick Richard for his patience and guidance throughout the course of this work. Thanks also goes to the members of my committee, Dr. Larry Weaver and Dr. Siegbert Hagmann, for the helpful suggestions and comments they offered concerning this work and to Dr. James McGuire for the many discussions concerning the theoretical aspect of this work.

I would also like to thank Justin Sanders, James Hall, Do-Hyung Lee, and Jeff Shinpaugh for their assistance in the data acquisition stage of this work.

A very special thanks goes to Wanda Henton for her patience and understanding during this work and also for saying "yes" when I asked her to marry me.

A final acknowledgement goes to the Division of Chemical Sciences, Office of Basic Energy Sciences, Office of Energy Research, U. S. Department of Energy for financial support of this work.

I. INTRODUCTION

Ion-atom collision processes have been studied with great interest over the past years and in recent years, a new area of collision studies concerning highly charged ions has developed with the availability of high energy accelerators.[1] Current advances in fusion technology have especially warranted increased study of atomic processes involving highly charged ions since at the high fusion temperatures, the particles in the plasma become highly charged due to collisions with hot electrons and interactions with other ions and atoms.[2] Collision processes of highly charged ions are also of considerable theoretical interest since the simpler systems of the highly charged ions are easier to model mathematically than many electron systems (i.e., atom-atom systems).[3] By experimentally measuring the probabilities of the occurrence of the several different atomic processes and comparing the experimental results to the results of theoretical calculations, we can determine the range of applicability of a particular theoretical model to accurately describe the physical processes taking place.

In an ion-atom collision, many single electron processes may occur. Some of these processes are electron capture by the projectile from the target atom, ionization of either or both the projectile and the target, and excitation of either or both the target and projectile. Collision systems of protons incident on highly charged one-electron ions would give results which are very easy to interpret due to the simplicity of the collision system (i.e., a three-body ion-ion

collision system). However, this study is very difficult to conduct experimentally since both the target and projectile are charged. A highly charged one-electron ion incident upon neutral atomic hydrogen closely approximates the three-body ion-ion collision. This experiment is also very difficult due to the need to produce a target of atomic hydrogen. In this thesis, the collision system of a highly charged ion incident upon a molecular hydrogen target is used to study the ionization of a one-electron, highly charged projectile by a target atom. The use of a molecular target makes the experimental procedure much less difficult, but it raises questions about how to handle a molecular target theoretically. The current theories used to describe ionization can handle atomic targets relatively well, however, no procedure for taking into account a molecular target has been developed.

Ionization is the process by which an electron is removed from an atom. In this work, the ionization of hydrogen-like oxygen and fluorine ions incident on a molecular hydrogen target over an energy range of 0.5 to 2.5 MeV/amu is studied. There is a considerable amount of data reported over this energy range for electron capture by highly charged ions,[4] however, there is relatively little ionization data. Dillingham[5] studied both capture and ionization processes for highly charged ions incident on helium over this energy range. The results of ionization of highly charged ions incident on a molecular hydrogen target of this work are compared to the results of ionization of highly charged ions incident on an atomic helium target by Dillingham.[5] The following illustrates a typical collision reaction.

$$O^{+7}(1s) + H_2 \longrightarrow O^{+8} + H_2^* + e^- \qquad (1.1)$$

The probability of the projectile ionization is measured by the "initial growth method."[5,6] The experimental procedure for measuring the ionization cross sections by this method is as follows. The incident hydrogen-like projectile beam is directed into a differentially pumped gas cell which contains the dilute target gas so that more than ninety percent of the original beam will pass through the gas cell without undergoing collisions. These conditions are maintained such that the projectiles will undergo "single collisions" with the target gas in the collision region. The fraction of the beam which does undergo collisions will change charge state depending on what collision process occurred. We determine the collision process which occured through observation of the charge changed beams. The beam emerging from the gas cell is magnetically analyzed to spacially separate the different charge states so that the ratios of number of particles in a particular charge state to the total number of particles can be measured to give the charge fractions of the beam. The charge fractions from a series of different target gas pressures are then fitted to a straight line using a least squares fitting routine. The slope of this function is multiplied by a normalization factor to give the ionization or capture cross section.

The following sections of this thesis discuss the development and current status of the Plane Wave Born Approximation and the Glauber Approximation which are the theories used to compare to the data of

this work. The experimental procedure is discussed in detail along with the data analysis techniques and conclusions from comparison of the theories with the data are presented in the final sections.

II. THEORY

As stated previously, ion-atom collisions are of considerable theoretical interest. In this work, we compare the experimental data with the Plane Wave Born Approximation[3,8,9] and the Glauber Approximation.[10] A summary of these theories follows.

a.) Plane Wave Born Approximation:

In the derivation of the Plane Wave Born Approximation (PWBA), consider the Schrodinger equation

$$\left(-\frac{\hbar^2}{2\mu}\nabla^2 + V\right)\psi = E\psi \tag{2.1}$$

which may be written

$$\left(\nabla^2 + k^2\right)\psi = U\psi \tag{2.2}$$

where $k^2 = \frac{2\mu E}{\hbar^2}$ and $U = \frac{2\mu V}{\hbar^2}$. The solution of the above equation is in terms of the Green's function[8]

$$G(\vec{R},\vec{R}') = \frac{\exp(ik|\vec{R}-\vec{R}'|)}{|\vec{R}-\vec{R}'|} \tag{2.3}$$

and is given by

$$\psi_k(\vec{R}) = \frac{1}{(2\pi)^{3/2}} e^{i\vec{k}\cdot\vec{R}} - \frac{1}{4\pi}\int G(\vec{R},\vec{R}')\, U(\vec{R}')\, \psi_k(\vec{R}')\, d^3R'. \tag{2.4}$$

At large distances, an approximation to the solution is

$$\psi_k(\vec{R}) \simeq \frac{1}{(2\pi)^{3/2}} e^{i\vec{k}\cdot\vec{R}} - \frac{e^{ikR}}{4\pi R}\int e^{-i\vec{k}'\cdot\vec{R}'}\, U(\vec{R}')\, \psi_k(\vec{R}')\, d^3R \tag{2.5}$$

where $\vec{k}$ is the beam direction and $\vec{k}'=k'\hat{R}$. This can be rewritten in terms of the scattering amplitude

$$f_k = -\frac{(2\pi)^{3/2}}{4\pi} \int e^{-i\vec{k}'\cdot\vec{R}'} U(\vec{R}') \psi_k(\vec{R}') d^3R' \tag{2.6}$$

as

$$\psi_k \simeq \frac{1}{(2\pi)^{3/2}} \left(e^{i\vec{k}\cdot\vec{R}} + \frac{e^{ikR}}{R} f_k\right). \tag{2.7}$$

The differential cross section for a particle scattered by the potential V can be written in terms of the scattering amplitude f_k as

$$\frac{d\sigma}{d\Omega} = |f_k|^2. \tag{2.8}$$

In the PWBA, the exact wave function $\psi_k(\vec{R}')$ in the expression for the scattering amplitude f_k is replaced by a plane wave. Thus, the scattering amplitude becomes

$$f_k \simeq \frac{-\mu}{2\pi\hbar^2} \int e^{-i\vec{k}'\cdot\vec{R}'} V(\vec{R}') e^{i\vec{k}\cdot\vec{R}'} d^3R'. \tag{2.9}$$

This approximation is valid assuming that the scattered particle behaves sufficiently like a free particle which has plane wave solutions to its Schrodinger equation.

For ionization of the electrons of a hydrogen-like atom, the exact wave functions are replaced by hydrogen-like wave functions multiplied by a plane wave. The scattering amplitude is now

$$f(q) = \frac{-\mu}{2\pi\hbar^2} \int \phi_f^*(\vec{r}) V \phi_i(\vec{r}) e^{i\vec{q}\cdot\vec{R}} d\vec{r}\, d\vec{R} \tag{2.10}$$

in terms of the momentum transfer $q=|\vec{k}-\vec{k}'|$, the electronic coordinate $\vec{r}$, and the internuclear coordinate $\vec{R}$.

The PWBA cross section can now be written, using atomic units, as

$$\sigma = \frac{1}{\mu^2 v^2} \int_{q_{min}}^{q_{max}} |f(q)|^2 q \, dq \tag{2.11}$$

where v is the relative velocity between the projectile and target. The minimum momentum transfer in the collision is

$$q_{min} = k - k'_{max} \simeq \frac{\Delta E}{2v} \left(1 + \frac{\Delta E}{2\mu v^2}\right) \simeq \frac{\Delta E}{2v} \tag{2.12}$$

where $k'_{max} = [2\mu(E-\Delta E)]^{1/2}$ and ΔE is the threshold energy of the process. If $\frac{\Delta E}{E} << 1$, the approximation for q_{min} is valid. With ΔE proportional to Z_2^2

$$q_{min} \simeq \frac{Z_2^2}{2v} . \tag{2.13}$$

The maximum momentum transfer in the collision

$$q_{max} = k + k'_{max} \simeq 2k . \tag{2.14}$$

This value is very large compared to q_{min} and may be taken to be infinity for mathematical convenience. Thus, the PWBA cross section becomes

$$\sigma = \frac{1}{\mu v^2} \int_{Z_2^2/2v}^{\infty} |f(q)|^2 q \, dq . \tag{2.15}$$

Using the Coulomb potential, the scattering amplitude becomes

$$f(q) = \frac{-\mu}{2\pi} \int \phi_i(\vec{r}) \frac{Z_1}{|\vec{r}-\vec{R}|} \phi_f(\vec{r}) \, e^{i\vec{q}\cdot\vec{R}} \, d\vec{r} \, d\vec{R} \, . \tag{2.16}$$

For one-electron ions of different atomic numbers, the hydrogen-like wave functions can be scaled in the following way.

$$\begin{aligned} r &\to \rho/Z_2 & d\vec{r} &= d\vec{\rho}/Z_2^3 \\ R &\to \mathcal{R}/Z_2 & & \\ \phi(\vec{r}) &= Z_2^{3/2}\phi(\vec{\rho}) & d\vec{R} &= d\vec{\mathcal{R}}/Z_2^3 \end{aligned} \tag{2.17}$$

The scaled scattering amplitude is

$$f(q) = \frac{-\mu}{2\pi} \int Z_2^{3/2} \, \phi_i(\vec{\rho}) \, \frac{Z_1 Z_2}{|\vec{\rho}-\vec{\mathcal{R}}|} \, Z_2^{3/2} \, \phi_f(\vec{\rho}) \, e^{i\vec{q}\cdot\vec{\mathcal{R}}/Z_2} \frac{d\vec{\rho}}{Z_2^3} \frac{d\vec{\mathcal{R}}}{Z_2^3} \, . \tag{2.18}$$

Thus, the scaled cross section becomes

$$\begin{aligned} \sigma &= \frac{Z_1^2}{Z_2^4} \int_{Z_2^2/2v}^{\infty} \left(\frac{f(q/Z_2)}{\mu}\right)^2 \frac{q}{v} \frac{dq}{v} \\ &= \frac{Z_1^2}{Z_2^4} \frac{1}{v^2} \int_{1/2v}^{\infty} \left(\frac{f(Q)}{\mu}\right)^2 Q \, dQ \end{aligned} \tag{2.19}$$

where $Q=q/Z_2$ and $V=v/Z_2$. Further reduction leads to

$$\begin{aligned} \sigma &= \frac{Z_1^2}{Z_2^4} \frac{F(V)}{V^2} \\ &= \frac{Z_1^2}{Z_2^4} F'(V) \end{aligned} \tag{2.20}$$

which is in terms of a universal function F'(V) scaled by a factor dependent only on the atomic numbers of the target and projectile.

The ionization cross section for a collision between a projectile of Z_1 and a target of Z_2 with relative velocity v_{inc} is

$$\sigma(Z_1,Z_2,v_{inc}) = \frac{Z_1^2}{Z_2^4}\,\sigma(1,1,v_{inc}/Z_2) \tag{2.21}$$

where $\sigma(1,1,v_{inc}/Z_2)$ is the ionization cross section for protons on hydrogen with relative velocity v_{inc}/Z_2. These cross sections have been calculated and are tabulated.[11,12]

Refinements to the original PWBA have come about in the form of correction factors due to different effects. Basbas et al.[13,14] have developed corrections for Coulomb deflection effects, increased binding effects, relativistic effects, and polarization effects.

A Coulomb deflection effect correction is necessary at lower projectile velocities. Usually, the projectile trajectory is assumed to be a straight line. But at low bombarding energies, the trajectory of the projectile is greatly influenced by the Coulomb field of the target atom. This causes the projectile to deviate from the straight line trajectory thus the correction is made by the use of a hyperbolic trajectory in the theoretical calculation instead of the straight line method.

The increased binding effect correction takes into account the increased binding energies of the target electrons when the projectile is inside the target atom K-shell radius. This increased binding causes the ionization cross section to decrease since the more tightly

bound electrons are less likely to be ejected from the target atom. This effect is most significant with lower energy projectiles because the slower moving projectiles spend a longer time within the target K-shell radius.

The correction for relativistic effects is simply the use of relativistic wave functions to describe the target electrons. The target electrons typically move at relativistic velocities, thus, the original PWBA using a non-relativistic description of the target electrons was inadequate. The use of this relativistic wave function gives a more accurate description of the target electrons, thus giving a more accurate theoretical prediction.

Corrections for polarization effects account for the reduced binding energy of the polarized target K-shell. When the projectile approaches the target atom, its electric field interacts with the target electrons causing the orbit of the target K-shell electrons to become distorted. The distortion results in a higher energy orbit which gives a lower binding energy. The lower binding energy allows an increase in the ionization cross section.

The PWBA calculations presented in this work are from a computer program developed by Rice[15] using the methods of Basbas including the corrections mentioned above.

b.) Glauber Approximation:

The Glauber Approximation is, in essence, a rigorous distorted-wave Born approximation.[16] It is an eikonal approximation using straight line trajectories. A brief derivation follows.[17]

Consider the Schrodinger equation

$$\left(\frac{-\nabla^2}{2M} + V\right)\psi = E\psi \ . \tag{2.22}$$

Letting $\psi = e^{i\vec{k}\cdot\vec{R}}\phi(R)$, the equation becomes

$$\left(\frac{k^2}{2M} + \frac{-\nabla^2}{2M} + \frac{-i\vec{k}\ \vec{\nabla}}{M} + V\right)\phi = E\phi \ . \tag{2.23}$$

Letting $k^2/2M = E$, $\hat{Z} = \hat{k}$, and assuming ϕ is slowly varying with respect to R,

$$\left(-iv\ \frac{d}{dz} + V\right)\phi = 0 \tag{2.24}$$

corresponding to the eikonal approximation

$$\psi = e^{i\vec{k}\cdot\vec{R}}\phi = e^{i\vec{k}\cdot\vec{R}}\ e^{\frac{i}{v}\int^Z V\ dZ'} \tag{2.25}$$

where ψ is a plane wave multiplied by an eikonal phase proportional to the average perturbing potential over the trajectory of the particle. The scattering amplitude from the above solution is

$$\begin{aligned} f &= \frac{-M}{2\pi}\int d\vec{k}\ e^{-i\vec{k}'\cdot\vec{R}}\ V\ \psi \\ &= \frac{-M}{2\pi}\int d\vec{R}\ e^{i(\vec{k}'-\vec{k})\cdot\vec{R}}\ V\ e^{\frac{i}{v}\int^Z V\ dZ'} \end{aligned} \tag{2.26}$$

which can be reduced further to the Glauber amplitude[17]

$$f(\vec{q},k_e) = \frac{-iM}{2\pi v}\int d^2B\ e^{i\vec{q}\cdot\vec{B}}\ \left(1 - e^{\frac{i}{v}\int_{-\infty}^{\infty} V\ dZ}\right) \ . \tag{2.27}$$

The ionization cross section is now

$$\sigma = \int |f(\vec{q},\vec{k}_e)|^2 \, d\vec{q} \, d\vec{k}_e \quad . \tag{2.28}$$

To account for the presence of electrons on the ionizing particle, a screened potential which behaves as the square of a momentum transfer dependent effective charge, $Z_1(q)$, may be used in the Glauber Approximation. For a one-electron particle, the expression for this screened potential is[18]

$$|Z_1(q)|^2 = |Z_1 - \phi_1(1s\text{-}1s;q)|^2 + 1 - |\phi_1(1s\text{-}1s;q)|^2 \tag{2.29}$$

which for hydrogenic wave functions becomes

$$|Z_1(q)|^2 = Z_1^2 + 1 - 2Z_1|1 + (q/2Z_1)^2|^{-2} \quad . \tag{2.30}$$

The Glauber Approximation using this screened potential is compared to the Glauber Approximation using a bare (Z_1^2) potential in the Results and Discussion section of this work.

The Glauber calculations presented in this work are from a computer program developed by Golden and McGuire.[16]

III. EXPERIMENTAL PROCEDURE

The experimental procedure for this study begins with an ion beam produced by one of the negative ion sources in the James R. Macdonald laboratory in the Kansas State University Physics Department. The beam is then accelerated by the KSU tandem Van de Graaff accelerator. The accelerated beam is magnetically analyzed by a 90° magnet, post stripped, and steered into the experimental beam line by a switching magnet (Fig. 1). In the experimental beam line, the beam passes through 4-jaw slits which are set to define a small beam and to cut down beam intensity so as not to damage the sensitive surface barrier detector. The beam then passes through the differentially pumped gas cell (Fig. 2) where collisions with the target gas take place. The beam emerging from the gas cell contains different charge states due to different collision processes. This beam is magnetically analyzed and the spacially separated charge state beams impinge on a position sensitive detector used in the experiment to detect the ions. The signals generated by the detector are amplified and fed into a computer where they are displayed as a spectrum and stored on magnetic disks for later analysis.

Two ion sources are available for use depending on whether the material used to make the projectile beam is solid or gaseous. The diode source is used for gaseous projectile materials and the sputter source is used for solid projectile materials.

In the diode ion source, an electrical arc is maintained in a hydrogen gas stream to produce a plasma where the gaseous projectile

Figure 1. Schematic diagram of the James R. Macdonald tandem Van de Graaff accelerator laboratory.

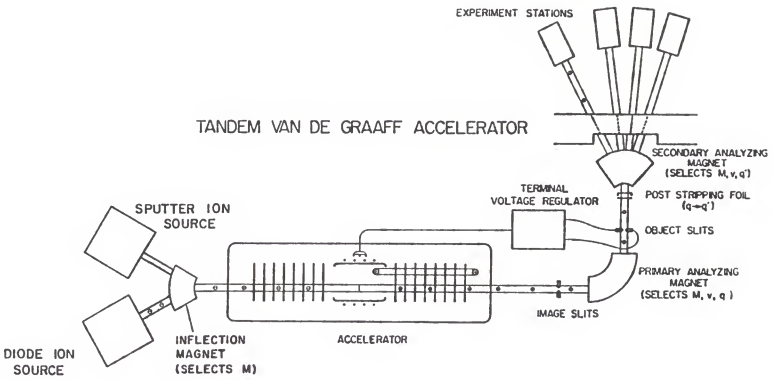
EXPERIMENT STATIONS
TANDEM VAN DE GRAAFF ACCELERATOR
SECONDARY ANALYZING MAGNET (SELECTS M, v, q')
TERMINAL VOLTAGE REGULATOR
POST STRIPPING FOIL (q→q')
SPUTTER ION SOURCE
OBJECT SLITS
PRIMARY ANALYZING MAGNET (SELECTS M, v, q)
IMAGE SLITS
DIODE ION SOURCE
INFLECTION MAGNET (SELECTS M)
ACCELERATOR

Figure 2. Schematic diagram of the experimental apparatus showing the target gas cell, target gas pressure control system, and the detector assembly.

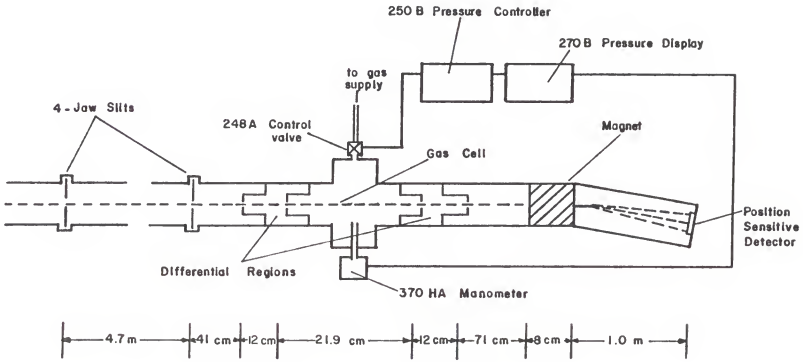
250 B Pressure Controller
270 B Pressure Display
to gas supply
4 - Jaw Slits
248A Control valve
Magnet
Gas Cell
Position Sensitive Detector
Differential Regions
370 HA Manometer
4.7 m
41 cm
12 cm
21.9 cm
12 cm
71 cm
8 cm
1.0 m

material is injected through a separate gas line. The projectile atoms are negatively charged in the plasma and are then extracted and accelerated toward the tandem Van de Graaff. In this study, sulfur hexafluoride (SF_6) was injected into the plasma to produce the fluorine ion beam.

In the sputter ion source, cesium vapor is ionized by a hot filament. These cesium ions are then accelerated onto a cathode containing the solid projectile material. The impact of the cesium ions "sputters" material from the cathode which then becomes negatively charged and is accelerated toward the tandem Van de Graaff. In this study, calcium fluoride (CaF_2) and aluminum oxide (Al_2O_3) were used to produce a fluorine ion beam and an oxygen ion beam.

The negative ion beam from either the sputter source or the diode source passes through an inflection magnet to select the desired species of ion to inject into the tandem Van de Graaff. The magnetically selected beam can be focused by an einzel lens and the position of the beam may be adjusted using electrostatic steerers just before entering the low energy end of the tandem Van de Graaff accelerator.

The negative ions enter the low energy end of the tandem Van de Graaff and are accelerated toward the positively charged terminal in the center of the accelerator. At the terminal, the ions pass through a stripping region in which a few electrons are removed from the ions so that they become positively charged. These positively charged ions are then repelled by the positively charged terminal and are accelerated out the high energy end of the tandem Van de Graaff.

The energy of the beam is varied by changing the positive potential on the terminal. The energy of the ion beam (in MeV) is determined by the relation

$$E=V(q+1)$$

where V is the positive potential on the terminal in MV and q is the charge state of interest in the beam emerging from the high energy end of the accelerator.

The stripping process produces a distribution of charge states in the beam emerging from the high energy end of the tandem Van de Graaff. This requires that, after focusing and steering of the beam on the high energy side of the accelerator, the ion beam be magnetically analyzed to select the desired charge state from this distribution. This is done with a 90° analyzing magnet.

To attain higher charge states than those which emerge from the accelerator, a thin carbon foil is placed in the beam path between the analyzing magnet and the switching magnet. This post stripping, like the terminal stripping, produces a distribution of charge states. The desired charge state of the post stripped ion beam is selected and steered into the experimental beam line by a switching magnet.

In the experimental beam line, the ion beam passes through two sets of 4-jaw slits. The first slit is set so that the intensity of the beam is reduced to less than 1000 particles per second. The extremely small opening needed to reduce the intensity to this level produces a highly directional point source of particles. The second set of 4-jaw slits is set to allow a nearly parallel beam of particles from the point source to enter the gas cell through the collimators.

Slight misalignment of the collimators will result in collisions between the particles in the beam and the edges of the collimators. The particles that collide with the collimator edges typically undergo charge exchange and become a contaminant beam entering the gas cell. Great care was taken to ensure that the collimators of the gas cell and the 4-jaw slits were properly aligned.

The differentially pumped gas cell (fig. 2) is defined by four optically aligned collimators, each with a 2 millimeter diameter aperture. The two outer regions of the gas cell are the differential regions which are maintained at a pressure of 1×10^{-6} torr or less during the experiment. The central region, which is 21.92 cm in length, is the collision region. The target gas is allowed to flow into the collision region through an MKS Baratron model 248A control valve which is activated by an MKS Baratron model 250B flow control unit. The flow controller compares the measured pressure in the collision region to the desired set point pressure and adjusts the valve to increase or reduce the flow of gas accordingly. The pressure in the collision region is measured by an MKS Baratron model 370HA capacitance manometer. The manometer sends a signal to an MKS Baratron model 270B signal conditioner which displays the pressure and sends a signal to the flow controller for the pressure comparison. The set pressure in the collision region is varied to get a pressure dependence which will be discussed later.

After collisions with the target gas, the beam comes out of the gas cell containing many charge states due to the different collision processes which took place. This beam is magnetically analyzed to

spacially separate the different charge states. The different charge state beams then impinge on an EG&G Ortec model P-055-0847-100 position sensitive surface barrier detector.

The detector produces two signals. One signal is proportional to the energy of the particle and the other is proportional to the position that the particle hit the detector. The raw signals from the detector are amplified by Ortec model 109PC pre-amplifiers. The signals are then amplified again by Canberra model 2020 spectroscopy amplifiers. The amplified analog position signals are converted to digital signals by a Canberra model 8070 analog-to-digital converter (ADC) and stored in the multichannel analyzer (MCA) of a Canberra Scorpio data acquisition system. The MCA sorts the signals according to pulse height which is proportional to the position that the particles hit the detector to form a position spectrum (Fig. 3). The height of a peak in the spectrum corresponds to the number of particles which hit the detector at that position.

To reduce the number of contaminant counts due to processes such as slit edge scattering, the ADC was gated. The energy signal from the spectroscopy amplifier is fed to an Ortec model 420A timing single channel analyzer (TSCA). The TSCA allows a "window" to be set such that signals which correspond to a particle with less energy than the lower limit on the window will not send a gate signal to the ADC. The ADC will then ignore the incoming position signal which corresponds to the particle with less energy.

The pressure dependence mentioned earlier is necessary to extract a cross section from the data. A pressure dependence is a series of

Figure 3. A typical spectrum for 32.25 Mev F^{+8} incident on molecular hydrogen gas at 35 millitorr.

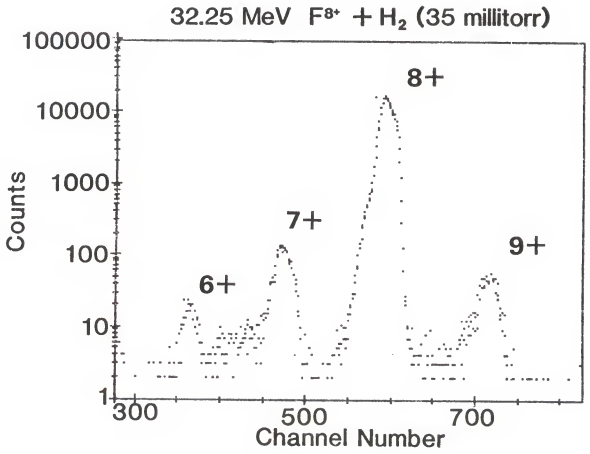
32.25 MeV F8+ + H2 (35 millitorr)
100000
10000
1000
100
10
1
Counts
6+
7+
8+
9+
300
500
700
Channel Number

spectra which are accumulated for the same collision system at different target gas pressures. For example, a 19 MeV F^{+8} beam incident on molecular hydrogen will have a pressure dependence series from zero pressure (background) to thirty-five millitorr in increments of five millitorr. Thus, there will be eight separate spectra, one for each target gas pressure.

IV. ANALYSIS

a.) Data Analysis:

As mentioned earlier, when the beam undergoes collisions with the target in the gas cell, it emerges containing several different charge states. The charge state composition of the beam can be described by the relative charge fractions

$$\phi_i = \frac{n_i}{\sum_i n_i} \tag{4.1}$$

where n_i is the number of particles in a given charge state i.

The change in charge state of the beam in collisions with the target can be described mathematically by

$$\frac{d\phi_i}{dx} = \sum_{j \neq i} (\sigma_{ji}\phi_j - \sigma_{ij}\phi_i) \tag{4.2}$$

where x is the target thickness and σ_{ij} is the charge exchange cross section for an atom going from charge state i to charge state j.

A solution to the above equation is

$$\phi_i = \phi_i(0) + \sum_{j \neq i} \sigma_{ji}x + \sum_{j \neq k} \sum_{k \neq i} \sigma_{jk}\sigma_{ki}x^2 + \ldots \quad . \tag{4.3}$$

An approximate solution to first order in target thickness is

$$\phi_i = \phi_i(0) + \sum_{j \neq i} \sigma_{ji}x \quad . \tag{4.4}$$

If processes which also populate the charge state of interest other than the primary process are ignored, the ionization cross section may be written as

$$\sigma_{\alpha i} = \frac{d\phi_i}{dx} \quad . \tag{4.5}$$

Therefore, the ionization cross section is simply the slope of the charge fraction ϕ_i versus the target thickness x.

Ignoring higher order terms to get this approximation to the cross section is valid in this study since "single collision conditions" were maintained. "Single collision conditions" criterion is that $\sigma N\ell < 0.1$[12] where σ is the largest cross section for charge change of the ion from the initial charge state, N is the number of target atoms per cm^3, and ℓ is the length of the target. For this study, ℓ is the length of the gas cell, which is constant, and σ is the projectile electron capture cross section and is also treated as a constant. Thus, N, the target density, is the only variable in this experimental set up. The target density is directly related to the target gas pressure, therefore, this condition allowed the calculation of the target gas pressure range which satisfied the "single collision conditions." A secondary check to the calculation is to plot the charge fractions versus the target gas pressure. If the charge fractions follow a linear path versus pressure, "single collision conditions" are satisfied. A typical charge fraction versus target pressure plot is shown in Figure 4.

Figure 4. A typical charge fraction versus target gas pressure plot for 15 MeV O^{+7} incident on molecular hydrogen.

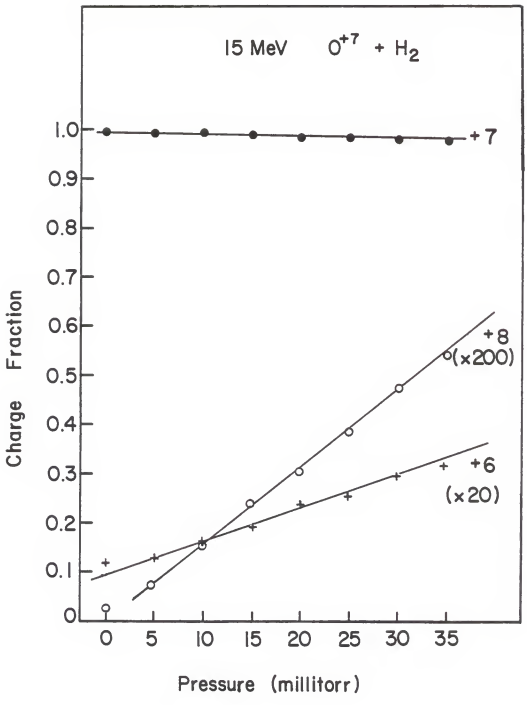
15 MeV O^{+7} + H_2
+7
+8
(x200)
+6
(x20)
Charge Fraction
1.0
0.9
0.8
0.7
0.6
0.5
0.4
0.3
0.2
0.1
0
0 5 10 15 20 25 30 35
Pressure (millitorr)

The approximation for the cross section requires the determination of the slope of the charge fractions versus the target thickness. So, the target gas pressure must be related to the target thickness. Using the ideal gas law, the relation

$$x = \frac{N_A}{RT} \ell P \tag{4.6}$$

is found where x is the target areal thickness in atoms per cm^2, N_A is Avagadro's number (6.02×10^{23} atoms per mole), R is the universal gas constant (8.313 J/mole·K), T is the temperature of the target gas in Kelvins, ℓ is the length of the target gas cell in cm, and P is the target gas pressure in millitorr.

The cross section can now be written as

$$\sigma_{\alpha i} = k \frac{d\phi_i}{dP} \tag{4.7}$$

where

$$k = \frac{RT}{N_A \ell} \tag{4.8}$$

is a constant for each cross section. The gas cell length was precisely measured and was constant throughout this work. The temperature was measured during each run and varied from one run to the next. This gave a different value of the constant k for each cross section. The values of k are tabulated in the appendix along with the calculated slopes.

To extract a cross section from the raw data, the number of counts in each peak in the spectrum is integrated to determine the charge fractions. The charge fractions versus target gas pressure are then fit to a straight line using the generalized least-squares algorithm of York.[19] The slope of this fitted line is then determined and multiplied by the constant k corresponding to that run to determine the cross section.

b.) Errors and Uncertainties:

Uncertainties of an experimentally measured quantity arise from limitations of the measuring devices and errors and approximations in the analysis of the measured quantity. In this study, uncertainties came from contaminant charge states in the incident beam, errors in the measurement of the target gas cell length and target gas pressure and temperature, efficiency of the detector, statistical errors, and errors in the calculation of the charge fractions and the slope of the charge fractions versus target gas pressure.

The uncertainties associated with the length of the gas cell, target gas pressure and target gas temperature were not major contributors to the overall error in the cross section measurement. The effective length of the gas cell had an uncertainty of approximately 2% due to the estimation of target gas flow through the collimators which defined the ends of the cell. The target gas pressure was measured very accurately and maintained very constant by the use of the flow control system described in the experimental section of this work. The error resulting from pressure uncertainties is negligible.

Uncertainties in measurement of the temperature of the target gas provided an additional one to two percent error.

Since the charge fractions are ratios, the error associated with absolute detector efficiency was eliminated. If the efficiency of the detector is constant across the entire sensitive area, the charge fractions do not depend on the absolute efficiency of the detector. The detector used in this experiment satisfies this condition unless damage occurs due to the intensity of the primary beam. By systematically varying the position where the charged particles struck the detector, damage from the intense primary beam was avoided.

Errors due to the analysis process are also very small. Calculation of the charge fraction has a small amount of error since the charge fraction is a sum over all states of the beam. Thus, an excited state is simply included into the sum over the charge state. In this study, the small error here is ignored. The errors in fitting the charge fraction versus target gas pressure to a line and calculating the slope of this line also produce small errors.

A possible systematic error is due to contaminant charge states in the incoming beam. These contaminant charge states are due to charge exchange in a collision with the edge of one of the slits used to define the beam. The slit-edge scattering effect is proportional to

$$\frac{t}{d} \tag{4.9}$$

where t is the thickness of the slit and d is the distance from the slit to the detector. In this study, methods for preventing this error were used as described in the experimental section of this work, but a method to precisely quantify this error was not developed.

V. RESULTS AND DISCUSSION

The results for ionization of hydrogen-like oxygen and fluorine ions incident on molecular hydrogen gas are given in Tables 1 and 2. The ionization cross sections are also plotted versus incident ion energy in Figure 5 with lines to guide the eye.

In Figures 6 and 7, the data of this work is compared to the projectile ionization cross sections of hydrogen-like oxygen and fluorine ions incident on helium targets from the work of Dillingham et al.[5] Selected helium target data points were repeated in this work to assure agreement between this work and the previous work. The molecular hydrogen target data falls approximately a factor of two below the helium target data consistently across this energy range. This agrees with a simple Born Approximation plus statistical scaling of the cross sections.

The experimental measurements are compared to theoretical calculations also. In Figures 8 and 9, the experimental data is compared to two versions of the Glauber approximation. The theoretical calculations are done for atomic hydrogen targets. The results are then multiplied by a factor of two and compared to the experimental ionization cross sections for projectiles incident on molecular hydrogen. The upper theoretical curve is the Glauber approximation using a screened nucleus potential for the hydrogen target. This is to account for the electron on the neutral hydrogen target. The lower curve corresponds to the Glauber approximation using a bare nucleus potential for the hydrogen target. The experimental cross sections

Table 1. Projectile ionization cross sections for O^{+7} + H_2 for various energies.

PROJECTILE IONIZATION CROSS SECTIONS FOR $O^{+7} + H_2$

ENERGY (MeV)	σ (X 10^{-19} cm^2)
8.0	0.54 ± 0.02
8.0	0.65 ± 0.02
10.0	0.81 ± 0.03
15.0	1.31 ± 0.05
15.0	1.00 ± 0.03
20.0	1.03 ± 0.03
25.0	1.31 ± 0.04
25.0	1.23 ± 0.04
25.0	1.29 ± 0.04
30.0	1.54 ± 0.05
35.0	1.55 ± 0.06

Table 2. Projectile ionization cross sections for F^{+8} + H_2 for various energies.

PROJECTILE IONIZATION CROSS SECTIONS FOR $F^{+8} + H_2$

ENERGY (MeV)	σ (X 10^{-20} cm^2)
9.5	1.39 ± 0.1
12.0	5.55 ± 0.2
12.0	3.13 ± 0.1
15.0	4.02 ± 0.1
15.0	5.03 ± 0.1
19.0	7.97 ± 0.2
22.0	7.28 ± 0.2
23.75	6.55 ± 0.2
27.0	7.96 ± 0.2
28.5	6.64 ± 0.3
33.25	7.63 ± 0.3
33.25	7.21 ± 0.2
38.0	7.73 ± 0.2
42.75	6.90 ± 0.2

Figure 5. Comparison of projectile ionization cross sections for $O^{+7} + H_2$ and $F^{+8} + H_2$. Lines are drawn to guide the eye.

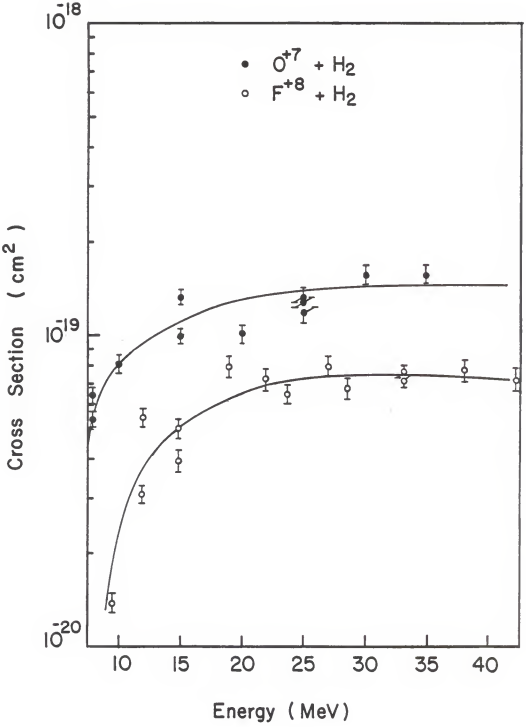
10^{-18}
10^{-19}
10^{-20}
Cross Section (cm^2)
O^{+7} + H_2
F^{+8} + H_2
10
15
20
25
30
35
40
Energy (MeV)

Figure 6. Comparison of projectile ionization cross sections for O^{+7} + H_2 and O^{+7} + He of this work and O^{+7} + He of Dillingham. Lines are drawn to guide the eye.

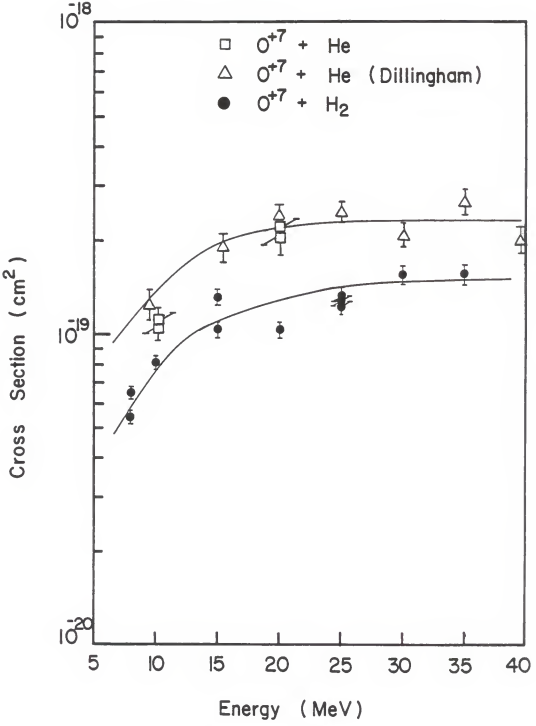
10^{-18}
10^{-19}
10^{-20}
Cross Section (cm^2)
O^{+7} + He
O^{+7} + He (Dillingham)
O^{+7} + H_2
5
10
15
20
25
30
35
40
Energy (MeV)

Figure 7. Comparison of projectile ionization cross sections for F^{+8} + H_2 of this work and F^{+8} + He of Dillingham. Lines are drawn to guide the eye.

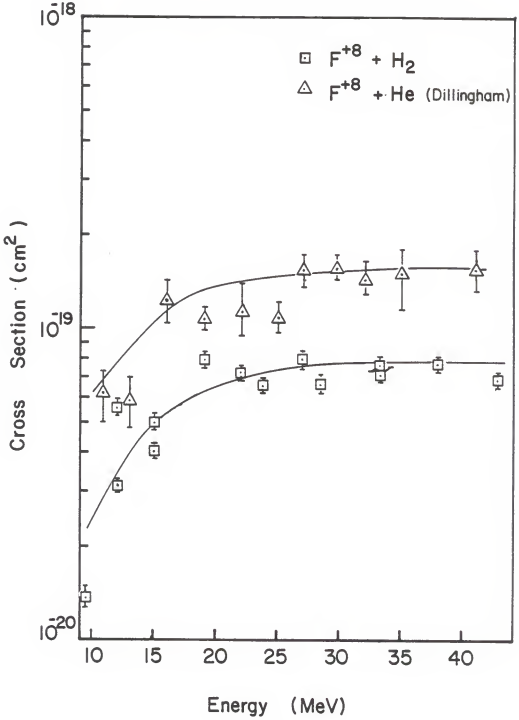
10^{-18}
10^{-19}
10^{-20}
Cross Section (cm^2)
$F^{+8} + H_2$
$F^{+8} + He$ (Dillingham)
10
15
20
25
30
35
40
Energy (MeV)

Figure 8. Comparison of projectile ionization cross sections for O^{+7} + H_2 with calculated projectile ionization cross sections for O^{+7} + H by the Glauber Approximation using a screened nucleus hydrogen potential and the Glauber Approximation using a bare nucleus hydrogen potential. The theoretical results are multiplied by two.

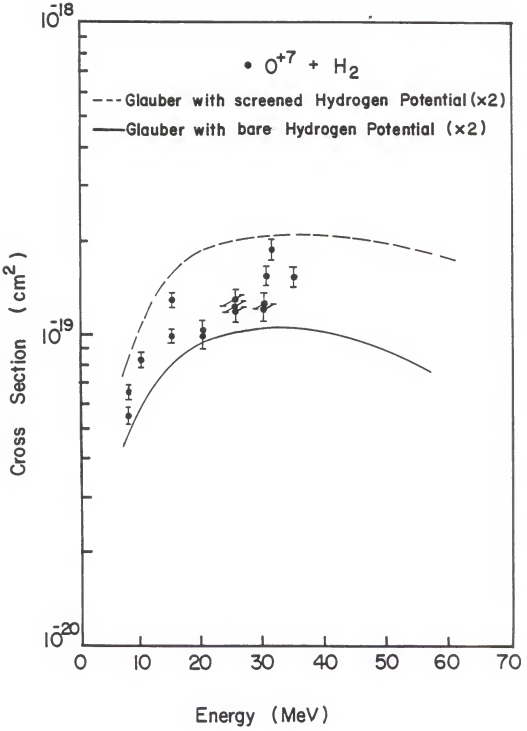
10^{-18}
10^{-19}
10^{-20}
• O^{+7} + H_2
---Glauber with screened Hydrogen Potential (x2)
—Glauber with bare Hydrogen Potential (x2)
Cross Section (cm^2)
0
10
20
30
40
50
60
70
Energy (MeV)

Figure 9. Comparison of projectile ionization cross sections for $F^{+8} + H_2$ with calculated projectile ionization cross sections for $F^{+8} + H$ by the Glauber Approximation using a screened nucleus hydrogen potential and the Glauber Approximation using a bare nucleus hydrogen potential. The theoretical results are multiplied by two.

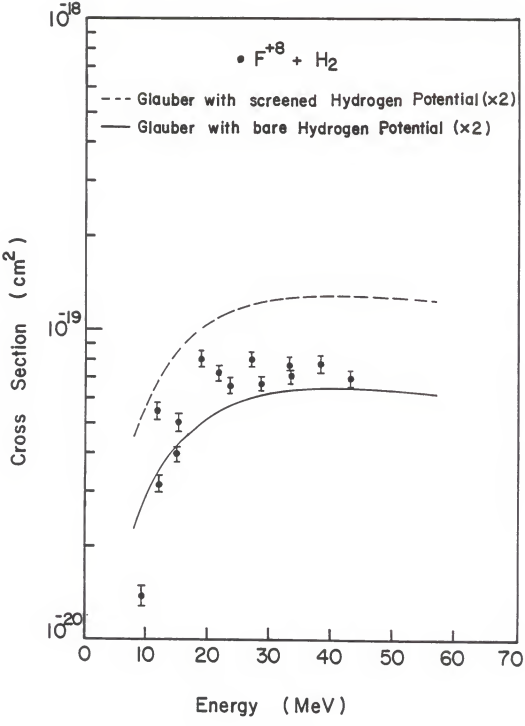
10^{-18}
10^{-19}
10^{-20}
• F^{+8} + H_2
--- Glauber with screened Hydrogen Potential (x2)
— Glauber with bare Hydrogen Potential (x2)
Cross Section (cm^2)
0
10
20
30
40
50
60
70
Energy (MeV)

fall between the two curves with the bare nucleus potential Glauber calculation showing better agreement in absolute magnitude with the data. The calculation using the screened nucleus potential suggests that the screening electrons of the target atom are approximately 60% more effective in ionizing the projectile than demonstrated by the data. However, both versions of the Glauber approximation have the same energy dependence which agrees with that of the experimental measurements.

In Figures 10 and 11, the experimental cross sections are compared to the Plane Wave Born Approximation (PWBA) both with and without the corrections mentioned in the theory section. Again the theoretical calculations have been done for atomic hydrogen and the results have been multiplied by two to compare to the molecular hydrogen target data. The dashed curve corresponds to the PWBA with increased binding, polarization effect, Coulomb effect, and relativistic effect corrections (PWBABPCR). The solid curve corresponds to the PWBA calculation without the correction factors. Both curves follow the energy dependence of the data, yet they overestimate the data. The PWBABPCR calculation is in better agreement in absolute magnitude with the data over the range studied here, especially at the lower energies.

As mentioned earlier, a technique for using the PWBA calculation involves scaling the calculation for protons incident on hydrogen by a factor z_1^2/z_2^4. This scaled PWBA is compared to the calculation using the Basbas techniques in Figures 12 and 13. The scaled PWBA falls significantly below the Basbas calculation. As a result, the scaled

Figure 10. Comparison of projectile ionization cross sections for O^{+7} + H_2 with calculated projectile ionization cross sections for O^{+7} + H by the Plane Wave Born Approximation (PWBA) and the Plane Wave Born Approximation with increased binding, polarization, Coulomb, and relativistic effects corrections (PWBABPCR). The theoretical results are multiplied by two.

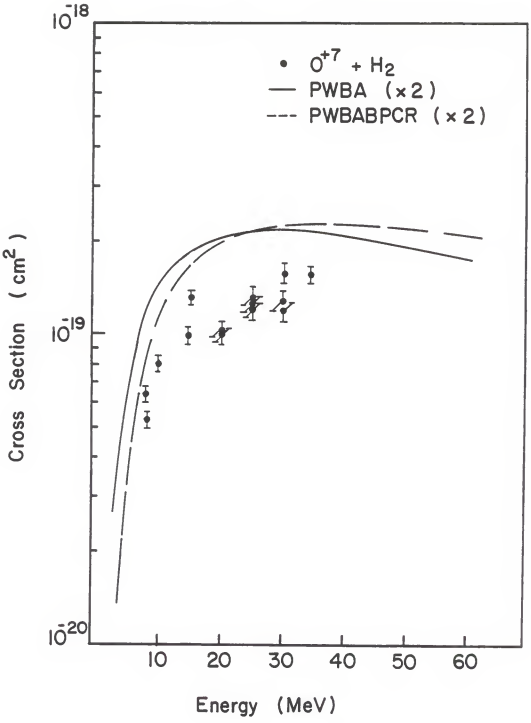
10^{-18}
10^{-19}
10^{-20}
Cross Section (cm^2)
• O^{+7} + H_2
— PWBA (×2)
--- PWBABPCR (×2)
10
20
30
40
50
60
Energy (MeV)

Figure 11. Comparison of projectile ionization cross sections for F^{+8} + H_2 with calculated projectile ionization cross sections for F^{+8} + H by the Plane Wave Born Approximation (PWBA) and the Plane Wave Born Approximation with increased binding, polarization, Coulomb, and relativistic effects corrections (PWBABPCR). The theoretical results are multiplied by two.

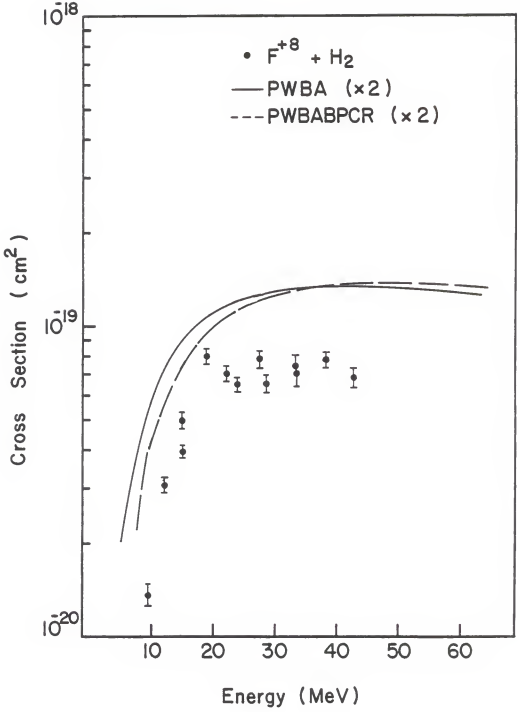
10^{-18}
10^{-19}
10^{-20}
• F^{+8} + H_2
—PWBA (×2)
---PWBABPCR (×2)
Cross Section (cm^2)
10
20
30
40
50
60
Energy (MeV)

Figure 12. Comparison of calculated projectile ionization cross sections for O^{+7} + H by the Basbas PWBA calculation and the scaled PWBA calculation. The theoretical results are multiplied by two.

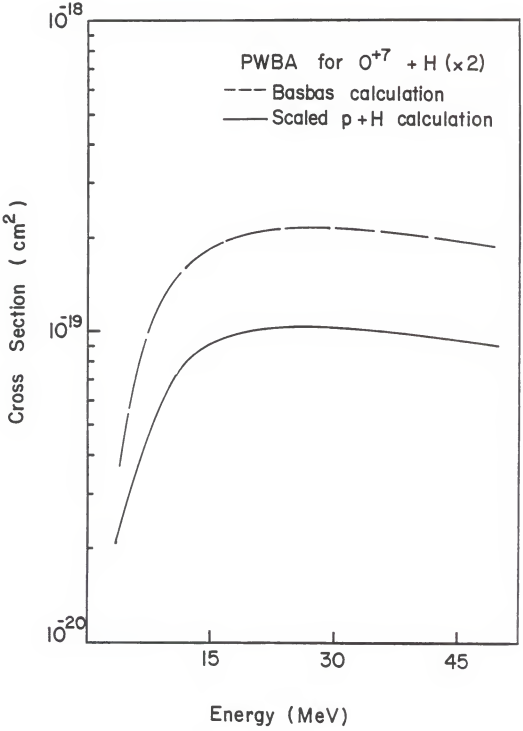
PWBA for O^{+7} + H (x2)
Basbas calculation
Scaled p + H calculation
10^{-18}
10^{-19}
10^{-20}
Cross Section (cm^2)
15
30
45
Energy (MeV)

Figure 13. Comparison of calculated projectile ionization cross sections for F^{+8} + H by the Basbas PWBA calculation and the scaled PWBA calculation. The theoretical results are multiplied by two.

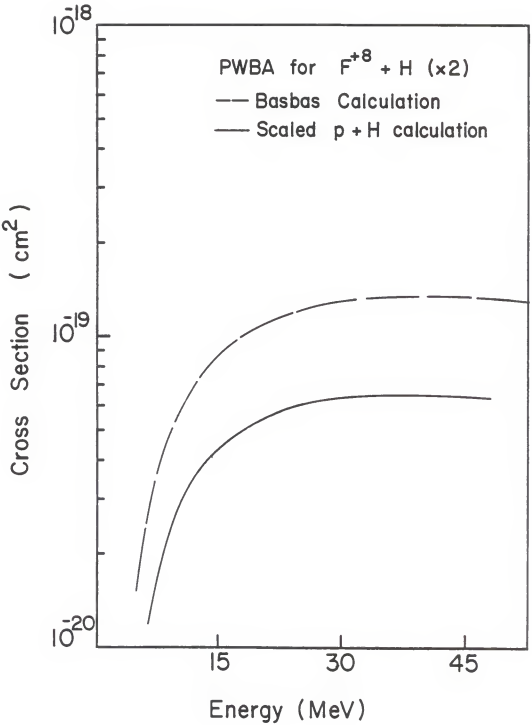
PWBA for F^{+8} + H (×2)
Basbas Calculation
Scaled p + H calculation
Cross Section (cm^2)
10^{-18}
10^{-19}
10^{-20}
15
30
45
Energy (MeV)

PWBA calculation agrees better with the data by sligthtly underestimating it. The scaled PWBA calculation gives results almost identical to the bare nucleus potential Glauber calculation for both the oxygen and fluorine projectile cases. Dillingham et al.[5] found that the scaled PWBA calculation agreed well with experiment for hydrogen-like ions incident on helium. A PWBA calculation using the Basbas techniques for hydrogen-like ions incident on helium was found to again be significantly greater than the scaled PWBA results.

A possible explanation of the discrepancy between the Basbas calculation and the scaled protons on hydrogen results is that the Basbas calculation assumes two K-shell electrons are present on the atom being ionized. The hydrogen-like ions used in this study have only one K-shell electron. If the Basbas calculation assumes two K-shell electrons present, dividing the results by two should bring the Basbas calculation into agreement with the scaled protons on hydrogen results. Figure 14 shows a comparison between the scaled protons on hydrogen results and the Basbas calculations divided by two. The agreement is excellent and seems to confirm the assumption of two K-shell electrons in the Basbas calculation.

In Figure 15, the PWBABPCR calculation is compared to the bare nucleus potential Glauber calculation. At high energies, the PWBABPCR is approximately a factor of two higher than the bare nucleus potential Glauber. However, at low energies, the two curves converge and show better agreement with the experimental data.

The technique for comparing the theoretical calculations to the experimental data by multiplying the atomic hydrogen calculations by a

Figure 14. Comparison of calculated projectile ionization cross sections for F^{+8} + H by the Basbas PWBA calculation and the scaled PWBA calculation. The results for the scaled PWBA are multiplied by two where the Basbas results are left in their original state since the assumption of two K-shell electrons introduces a factor of two into the calculation.

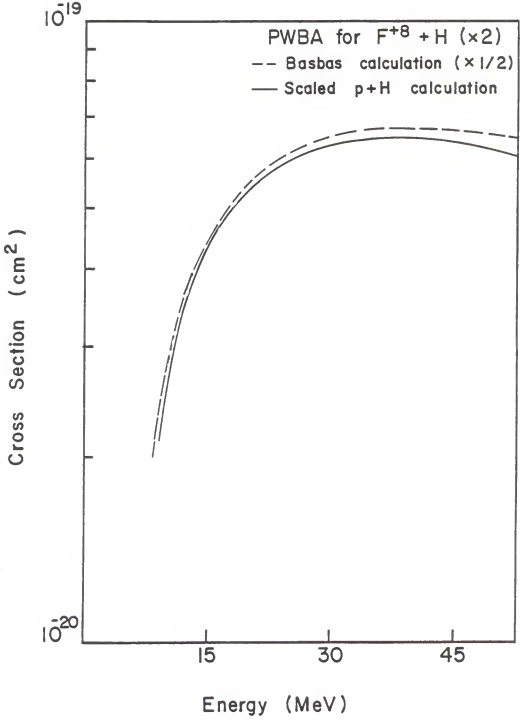
PWBA for F^{+8} + H (×2)
-- Basbas calculation (× 1/2)
— Scaled p+H calculation
10^{-19}
10^{-20}
Cross Section (cm^2)
15
30
45
Energy (MeV)

Figure 15. Comparison of calculated projectile ionization cross sections for F^{+8} + H by the Basbas PWBABPCR and the Glauber Approximation using a bare nucleus hydrogen potential. The theoretical results are multiplied by two.

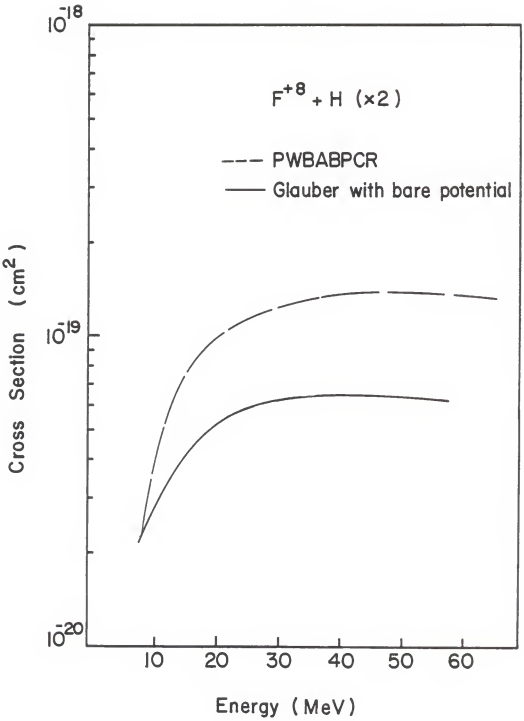
10^{-18}
10^{-19}
10^{-20}
Cross Section (cm^2)
F^{+8} + H (×2)
PWBABPCR
Glauber with bare potential
10
20
30
40
50
60
Energy (MeV)

factor of two assumes, in essence, that the molecular hydrogen target behaves as if it were two atomic hydrogen targets. Better agreement between theory and experiment may be achieved by developing a calculational method which will allow a molecular hydrogen target to be included in the theory.

VI. SUMMARY

Cross sections were measured for projectile ionization of hydrogen-like oxygen and fluorine ions incident on a molecular hydrogen target. The experimental cross sections are arrived at by taking the slope of a fitted line to the charge fractions of a pressure dependence and multiplying the slope by a normalization factor.

The experimental cross sections are compared to various theoretical calculations. No method for including a molecular target has been developed for the theories used in this study, therefore, the calculations were performed for atomic hydrogen targets, then multiplied by two. The comparison showed that the PWBA and PWBABPCR by Rice and the screened nucleus potential Glauber approximation give similar results which overestimate the data by as much as 60%. However, dividing the PWBA and PWBABPCR by two to account for the assumption of two K-shell electrons, as mentioned in the previous section, brings the results into much better agreement with the data. The scaled PWBA and the bare nucleus potential Glauber approximation give almost identical results and agree very well with the data, but still underestimate the data by about ten to twenty percent.

Better agreement between experiment and theory may be obtained if a method for using a molecular target in the theoretical calculations is developed. This would eliminate the need to assume that the molecular hydrogen target behaves as two atomic hydrogen targets.

Since the Glauber approximation using a bare nucleus potential agrees best with the experimental data, this might imply that the highly charged incoming projectile removes the electrons from the neutral target before the target ionizes the projectile. Further study of the explicit effects of the target electrons may provide a better understanding of this process.[20]

As mentioned earlier, a possible error is due to the summation over all states of the charge state beams to determine the charge fractions. By separating the excited states from the summation, the cross section measurement may be improved.

REFERENCES

1) P. Richard, in Atomic Inner-Shell Processes, edited by B. Craseman (Academic Press, New York, 1975), Vol. 1, pp. 74-152.

2) C. F. Barnett, invited lecture IX ICPEAC, 1975, The Physics of Electron and Atomic Collisions, edited by J. S. Risley and R. Geballe, pp. 846-853.

3) M. R. C. McDowell and J. P. Coleman, Introduction to the Theory of Ion-Atom Collisions, (North-Holland, Amsterdam, 1970), Chap. 7.

4) H. Knudsen, H. K. Haugen, and P. Hvelplund, Phys. Rev. A24, 2287 (1981).

5) T. R. Dillingham, J. R. Macdonald, and Patrick Richard, Phys. Rev. A24, 1237 (1981).

6) T. Chiao, Ph.D. Thesis (Kansas State University, 1973).

7) J. R. Macdonald and F. W. Martin, Phys. Rev. A4, 1965 (1971).

8) E. Merzbacher, Quantum Mechanics, (John Wiley and Sons, Inc., New York, 1970), Chap. 11.

9) D. R. Bates, in Atomic and Molecular Processes, edited by D. R. Bates (Academic Press, New York, 1962), pp. 549-621.

10) R. J. Glauber, Lectures in Theoretical Physics, edited by W. E. Brittin and L. G. Dunham, (Interscience, New York, 1959), Vol. 1, pp. 315-414.

11) J. E. Golden, Ph.D. Thesis (Kansas State University, 1975).

12) T. R. Dillingham, M.S. Thesis (Kansas State University, 1980).

13) G. Basbas, W. Brandt, and R. Laubert, Phys. Rev. A7, 983 (1973).

14) G. Basbas, W. Brandt, and R. Laubert, Phys. Rev. A17, 1655 (1978).

15) R. Rice, private communication.

16) J. E. Golden and J. H. McGuire, Phys. Rev. Letters 32, 1218 (1974).

17) J. H. McGuire, Phys. Rev. A26, 143 (1982).

18) J. H. McGuire, N. Stolterfoht, and P. R. Simony, Phys. Rev. A24, 97 (1981).

19) D. York, Canadian Journal of Physics 44, 1079 (1966).

20) J. H. McGuire, private communication.

APPENDIX

The following table lists the filenames of the data presented in this work, the slope of the fitted line to the charge fractions, and the normalization constant, k, corresponding to each data point. The choice of the filename is illustrated by the following example.

2375F8H229Y

The leading numbers in the filename designate the projectile energy in MeV. A decimal point is assumed after the first two numbers so that the first two numbers designate units of MeV and any numbers following are a decimal fraction of an MeV. In the above example, the projectile energy is 23.75 MeV. After the leading numbers, a letter followed by a number designates the ion beam species and charge state. In the example given, F8 designates a F^{+8} ion beam. Following the beam identification is the target specification. In the example given, H2 designates a molecular hydrogen target (H_2). The last three characters (two numbers followed by a letter) designate the page in Richard Data Book 15 which contains the raw data. The letter will be either W or Y corresponding to a white (W) page or a yellow (Y) page. The numbers are simply the page number. In the example, the raw data may be found on the yellow page 29.

Table A1. Filename, slope, and normalization constant, k, for the experimental data of this work.

Filename	Slope ($X\ 10^{-5}$)	k ($X\ 10^{-15}$)
0807H247Y	4.0 ± 0.1	1.35
0807H248W	4.78 ± 0.10	1.35
1007H242Y	6.01 ± 0.10	1.35
1507H244Y	9.5 ± 0.3	1.37
1507H246Y	7.33 ± 0.04	1.37
2007H240Y	7.66 ± 0.01	1.35
2507H246W	9.6 ± 0.1	1.37
2507H252W	9.17 ± 0.08	1.34
2507H252Y	9.67 ± 0.05	1.34
3007H253W	11.52 ± 0.06	1.34
3507H253Y	11.6 ± 0.3	1.34
095F8H232Y	0.99 ± 0.08	1.40
12F8H254W	4.15 ± 0.03	1.34
12F8H254Y	2.33 ± 0.01	1.34
15F8H223W	2.95 ± 0.02	1.36
15F8H232W	3.61 ± 0.01	1.39
19F8H228Y	5.87 ± 0.04	1.36
22F8H237Y	5.39 ± 0.06	1.35
2375F8H229Y	4.82 ± 0.09	1.36
27F8H230W	5.86 ± 0.02	1.36
285F8H230Y	4.89 ± 0.2	1.36
3325F8H231W	5.62 ± 0.2	1.36
3325F8H233W	5.17 ± 0.1	1.39
38F8H233Y	5.54 ± 0.07	1.39
4275F8H234W	4.94 ± 0.1	1.40

PROJECTILE IONIZATION OF HYDROGEN-LIKE OXYGEN AND FLUORINE IONS INCIDENT ON MOLECULAR HYDROGEN

by

TRACY NOLAN TIPPING

B.S., East Texas State University, 1984

AN ABSTRACT OF A MASTER'S THESIS

submitted in partial fulfillment of the

requirements for the degree

MASTER OF SCIENCE

Department of Physics

KANSAS STATE UNIVERSITY
Manhattan, Kansas

1986

ABSTRACT

Cross sections for projectile ionization have been measured using the "initial growth method" for hydrogen-like oxygen and fluorine ions incident on a molecular hydrogen target over a projectile energy range of 0.5 to 2.5 MeV/amu. The measured projectile ionization cross sections for hydrogen-like ions incident on molecular hydrogen are approximately a factor of two smaller than the projectile ionization cross sections for hydrogen-like ions incident on helium measured by Dillingham et al. This agrees with a simple Born Approximation plus statistical scaling of the cross sections. The experimental data is compared to the Plane Wave Born Approximation (PWBA) and the Glauber Approximation. The PWBA calculations both with and without corrections for increased binding, Coulomb deflection, polarization, and relativistic effects show similar projectile energy dependence as the experimental data but overestimate the data. The Glauber Approximation using a screened nucleus potential for the hydrogen target also overestimates the data. The Glauber Approximation using a bare nucleus potential for the hydrogen target shows similar projectile energy dependence to the data as does the screened potential case, but underestimates the data slightly. It was semiempirically determined that the Glauber Approximation using a bare nucleus potential must be multiplied by 1.25 to agree with the data and the Glauber Approximation using a screened nucleus potential must be multiplied by a factor of 0.65 to bring it into agreement with the data. The latter

calculation suggests that the screening electrons of the target atom are approximately 60% more effective in ionizing the projectile than demonstrated by the data.